Global Horizontal Irradiance in West Africa: Evaluation of the WRF-Solar Model in Convection-Permitting Mode with Ground Measurements

Windmanagda Sawadogo,[a] Jan Bliefernicht,[a] Benjamin Fersch,[b] Seyni Salack,[c] Samuel Guug,[c] Kehinde O. Ogunjobi,[c] Stefanie Meilinger,[d] and Harald Kunstmann[a,b]

[a] Institute of Geography, University of Augsburg, Augsburg, Germany
[b] Institute of Meteorology and Climate Research (IMK-IFU), Karlsruhe Institute of Technology, Garmisch-Partenkirchen, Germany
[c] West African Science Service Centre on Climate Change and Adapted Land Use Competence Centre, Ouagadougou, Burkina Faso
[d] International Centre for Sustainable Development (IZNE), University of Applied Sciences Bonn-Rhein-Sieg, Sankt Augustin, Germany

ABSTRACT: The number of solar power plants has increased in West Africa in recent years. Reliable reanalysis data and short-term forecasting of solar irradiance from numerical weather prediction models could provide an economic advantage for the planning and operation of solar power plants, especially in data-poor regions such as West Africa. This study presents a detailed assessment of different shortwave (SW) radiation schemes from the Weather Research and Forecasting (WRF) Model option Solar (WRF-Solar), with appropriate configurations for different atmospheric conditions in Ghana and the southern part of Burkina Faso. We applied two 1-way nested domains (D1 = 15 km and D2 = 3 km) to investigate four different SW schemes, namely, the Community Atmosphere Model, Dudhia, RRTMG, Goddard, and RRTMG without aerosol and with aerosol inputs (RRTMG_AERO). The simulation results were validated using hourly measurements from different automatic weather stations established in the study region in recent years. The results show that the RRTMG_AERO_D01 generally outperforms the other SW radiation schemes to simulate global horizontal irradiance under all-sky condition [RMSE = 235 W m^{-2} (19%); MAE = 172 W m^{-2} (14%)] and also under cloudy skies. Moreover, RRTMG_AERO_D01 shows the best performance on a seasonal scale. Both the RRTMG_AERO and Dudhia experiments indicate a good performance under clear skies. However, the sensitivity study of different SW radiation schemes in the WRF-Solar model suggests that RRTMG_AERO gives better results. Therefore, it is recommended that it be used for solar irradiance forecasts over Ghana and the southern part of Burkina Faso.

KEYWORDS: Africa; Shortwave radiation; Climate models; Renewable energy

1. Introduction

The generation of electricity from solar radiation has increased worldwide in recent decades. According to the International Energy Agency (IEA), solar photovoltaic (PV) electricity generation is the technology with the largest absolute growth rates in electricity generation among renewable energy technologies (IEA 2018). Furthermore, the affordability and availability of solar PV technology could be an opportunity for many developing countries in subtropical and tropical regions like West Africa to expand their electricity generation to better meet the electricity needs of their populations.

West African countries are still struggling with electricity security, and renewable energies like solar PV technologies can help improve electricity supply. For instance, Ghana has a total installed capacity of 4399 MW, mainly from hydropower (1580 MW) and thermal power plants (2796 MW), while energy generated from solar and wind is still negligible (22.5 MW). Like many other West African countries, Ghana has an estimated access electricity of more than 80%, but about

1.2 million households still live without electricity (U.S. Agency for International Development 2020). Despite progress in electricity supply in recent decades, West African countries still face electricity shortages. This situation contributed to a 2% loss of annual GDP in Ghana for the year 2014 (Kumi 2017). To overcome these problems, Ghana, for example, intends to scale up the share of renewable energy to 10% by 2030, and solar energy technologies could contribute significantly to achieving this goal. Grid-integrated PV systems and stand-alone PV hybrid systems could improve electricity security in the country. However, for the expansion of solar PV technologies, accurate information on solar resources is needed to better quantify and forecast the potentials in this challenging region. The Energy-Self-Sufficiency for Health Facilities in Ghana (ENERSHELF) project aims to use solar radiation forecasts and reanalysis to improve the operation of PV hybrid systems in Ghana.

The estimation of solar energy yields requires reliable information on solar irradiance at specific locations. In situ data from weather stations are the most accurate source for this purpose. However, the network of weather stations in Africa is sparsely distributed (Dike et al. 2018). For this reason, in data-poor regions, information from numerical weather prediction (NWP) models, satellite-based datasets, and reanalysis data is often used to derive spatially homogeneous solar radiation data for a geographical region of interest (Sawadogo et al. 2020; Neher et al. 2019). Reliable solar radiation estimation

---

Corresponding author: Windmanagda Sawadogo, windmanagda.sawadogo@geo.uni-augsburg.de

from these approaches remains challenging due to the uncertainties in aerosol optical depth (AOD; Neher et al. 2019) and cloud optical properties resulting from uncertainties in cloud microphysical properties in the model (Troccoli and Morcrette 2014). These uncertainties are associated with the specific algorithms, cloud type, or shortwave (SW) radiation schemes used in the NWP, satellite-based observation, and reanalysis datasets (Lee et al. 2016; Quaas et al. 2009).

NWP simulations are used to assess the sensitivity of solar radiation and other weather variables. State-of-the-art models such as the Weather Research and Forecasting (WRF) Model provide different types of parameterization schemes like shortwave and longwave (LW) radiation schemes, and the best scheme can be selected for a study region of interest. For instance, Zempila et al. (2016) used four different WRF radiation schemes [Dudhia, updated Rapid Radiative Transfer Model for GCMs (RRTMG), updated Goddard, and the Geophysical Fluid Dynamics Laboratory (GFDL)] to evaluate the global horizontal irradiance (GHI) for Greece with ground measurements. Their study showed that the Dudhia scheme performed best under clear skies. Chen et al. (2017) also showed that the Dudhia scheme performed better when simulating GHI over Xinjiang in China under clear skies. The RRTMG scheme in the WRF Model shows a good performance in simulating GHI and direct normal irradiance (DNI) when aerosol inputs are supplied, but the authors suggest that the Dudhia scheme better reproduces the solar radiation components under clear skies (Ruiz-Arias et al. 2013).

In recent years, the WRF Model has been further developed for solar energy applications. This WRF version is called WRF-Solar. The WRF-Solar model is built upon the WRF Model developed by the National Center for Atmospheric Research (NCAR) and was designed for solar energy applications (Jiménez et al. 2016b). Compared with the standard WRF Model, WRF-Solar provides reliable solar irradiance forecasting with an improved representation of aerosol–radiation feedbacks. WRF-Solar also accounts for cloud–aerosol feedbacks and enables a fully coupled aerosol–cloud–radiation system with time-varying aerosol inputs. Numerous studies have thoroughly evaluated the WRF-Solar model for forecasting applications (Yang et al. 2021; Balog et al. 2019; Kim et al. 2017). These studies show that solar radiation forecasts with WRF-Solar can contribute to better solar resource planning. For instance, Sosa-Tinoco et al. (2022) used the WRF-Solar model to forecast GHI in two power plants in Spain. The authors suggest that including aerosols in the model improves the forecast by 10%. Jiménez et al. (2022) also used the WRF-Solar model to evaluate the performance of the GHI forecast over the contiguous United States (CONUS). The model is also used for model development (Cheng et al. 2022; Prasad and Kay 2020).

NWP models like WRF and its derivatives such as the WRF Model coupled with chemistry (WRF-Chem) and the WRF hydrological modeling system (WRF-Hydro) have been frequently used for different purposes in West Africa but have received less attention for solar energy applications. For instance, Klein et al. (2015) used a WRF multiphysics ensemble to analyze the effect of parameterization schemes on precipitation and West African monsoon features. Another study investigated the influence of parameterization on precipitation associated with the African easterly waves by combining 62 configuration physics of the WRF Model (Noble et al. 2014). Gbode et al. (2019) analyzed the effect of parameterization of the WRF Model on precipitation and surface temperature with 27 different physics combinations during the monsoon regime for the year 2017. Oluleye and Folorunsho (2019) used WRF-Chem to investigate the impact of the African easterly jet on dust transport over the region. Another WRF-Chem study evaluated dust events in the Sahel region using station data (Gueye and Jenkins 2019). WRF-Hydro has been used to simulate runoff and other hydrological variables in different catchments in West Africa (Quenum et al. 2020; Naabil et al. 2017; Arnault et al. 2016) and to evaluate different physics schemes within the model (Arnault et al. 2021). These studies have focused almost exclusively on the sensitivity of parameterization on the West African monsoon associated with its different drivers and on the runoff and aerosol simulations in the region, but not on solar radiation.

The objective of this study was to comprehensively evaluate a state-of-the-art NWP model for solar energy applications in West Africa. We use four different shortwave radiation schemes from the latest version of WRF-Solar, including time-varying aerosols. The motivation behind this approach is to select the best shortwave radiation scheme for solar irradiance forecasting in the region. Simulations are driven from reanalysis information in high spatiotemporal resolution (31 km, 1 h), focusing on Ghana and southern Burkina Faso. For the analysis, we make use of subhourly GHI measurements from novel networks of automatic weather stations (AWSs) established as part of the West African Science Service Centre on Climate Change and Adapted Land Use (WASCAL) program (Salack et al. 2019; Bliefernicht et al. 2018) and by the Ghana Meteorological Agency (GMet). This study is therefore one of the first to use the information from these different AWS networks.

The paper is organized as follows. Section 2 provides a brief description of the WRF-Solar model, the modeling experiments, and different datasets used in this study. Section 3 presents the results and discussion of the main evaluations of GHI across different locations. Section 4 presents the conclusion of the study.

2. Experiments, data, and methods

a. Model configuration and setup

We used WRF-Solar, version 4.2.1, with two 1-way nested domains over West Africa for different configurations. The outer domain (D1) extends from 5°S to 30°N and from 23°W to 23°E with a spatial resolution of 15 km with 299 × 219 grid points, while the inner domain (D2) covers an area from 1° to 14.5°N and from 10°W to 8.5°E with a spatial resolution of 3 km with 600 × 400 grid points (Fig. 1). The initial and lateral boundary conditions (ILBC) were taken from the European Centre for Medium-Range Weather Forecasts (ECMWF) hourly ERA5 reanalysis data (Hersbach et al. 2020). The model first simulates domain D1 with the ERA5 reanalysis
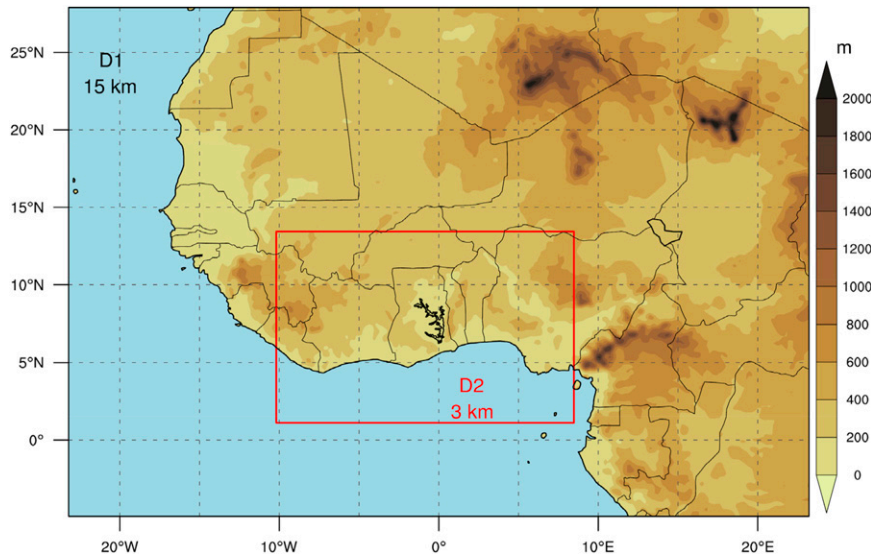
FIG. 1. WRF domains scaled by the topography of the region. The black-outlined rectangle shows the outer domain (D1) with a grid spacing of 15 km, whereas the red-outlined rectangle shows the inner domain (D2) with a horizontal resolution of 3 km.

as ILBC and then creates new output data (which are temporally and spatially interpolated) and serves as ILBC for domain D2 without feedback. Both domains cover the location of the different AWSs used in this study (cf. Fig. 1 with Fig. 2). For the WRF Preprocessing System (WPS), we used the land use index and land use fraction from the 21-class Moderate Resolution Imaging Spectroradiometer (MODIS) and the green vegetation index from the Fraction of Photosynthetically Active Radiation (FPAR). The GEODATA TOPO 10 M for the U.S. Geological Survey (USGS) topography data were used to initialize the land use in the model.

b. Modeling experiment

The model used 45 levels of terrain-following eta layers from the surface (1000 hPa) to 50 hPa. For the physics parameterizations of the model, many factors are considered. Clouds and aerosols are the largest areas of uncertainty in climate simulations, and high biases increase when coupled with different radiation schemes (Thompson et al. 2016). The parameterization of resolved clouds and precipitation in climate models is done through the microphysics scheme. The WRF Model provides 21 microphysics schemes, each of which has its own characteristics. Based on recent studies with the WRF-Solar model, the Thompson microphysics scheme is preferred (Yang et al. 2021; Prasad and Kay 2020; Jiménez et al. 2016b). This scheme predicts the mixing ratios of the five hydrometeor classes (cloud water, rain, snow, graupel, and cloud ice) and the number of concentrations of cloud. The effective radii of ice, snow, and cloud water computed in the routine Thompson microphysics scheme are subsequently passed to the radiation scheme (Thompson et al. 2016).

The feedback from clouds to shortwave radiation is done through the cumulus scheme. However, clouds are underrepresented at the subgrid scale in many of these schemes. The effects of unresolved clouds are important in solar irradiance forecasting using the WRF-Solar model (Jiménez et al. 2016a). To enhance the representation of unresolved clouds, we chose Deng's shallow cumulus parameterization (Deng et al. 2014). In other words, we turned off the cumulus scheme and used the shcu_physics = 5 option in the WRF namelist to account for the Deng scheme for D1 (15 km). However, at high resolution, the microphysics scheme is able to explicitly develop convection on the model grid without the cumulus scheme. Nonetheless, a recent study by Jiménez et al. (2022) has shown that using Deng's shallow cumulus parameterization improves the solar irradiance forecasts even at high resolution when the model is run in convection-permitting mode over the CONUS domain. Therefore, we also enabled the effect of unresolved clouds on the shortwave radiation for D2 (3 km).

In addition, the call of the radiative parameterization is crucial for the computational time. The Fast All-Sky Radiation Model for Solar Applications (FARMS) shortens the computational time by avoiding computing three-dimensional heating rates and gives more accurate values for the solar radiation components at each model time step compared with the traditional radiative transfer model (Xie et al. 2016). In this study, we used the GHI of FARMS in the WRF-Solar model. Another physics scheme that is important for solar energy applications is the land surface model (LSM), as it accounts for subgrid fluxes on the ground. The LSM simulates the water and energy exchange between the land surface model and the atmosphere and performs, therefore, the partitioning between latent heat, sensible heat, and ground heat fluxes. For better representation of land surface fluxes in the model, we selected the Noah land surface model (Niu et al. 2011). The surface fluxes and cloud formation depend on the
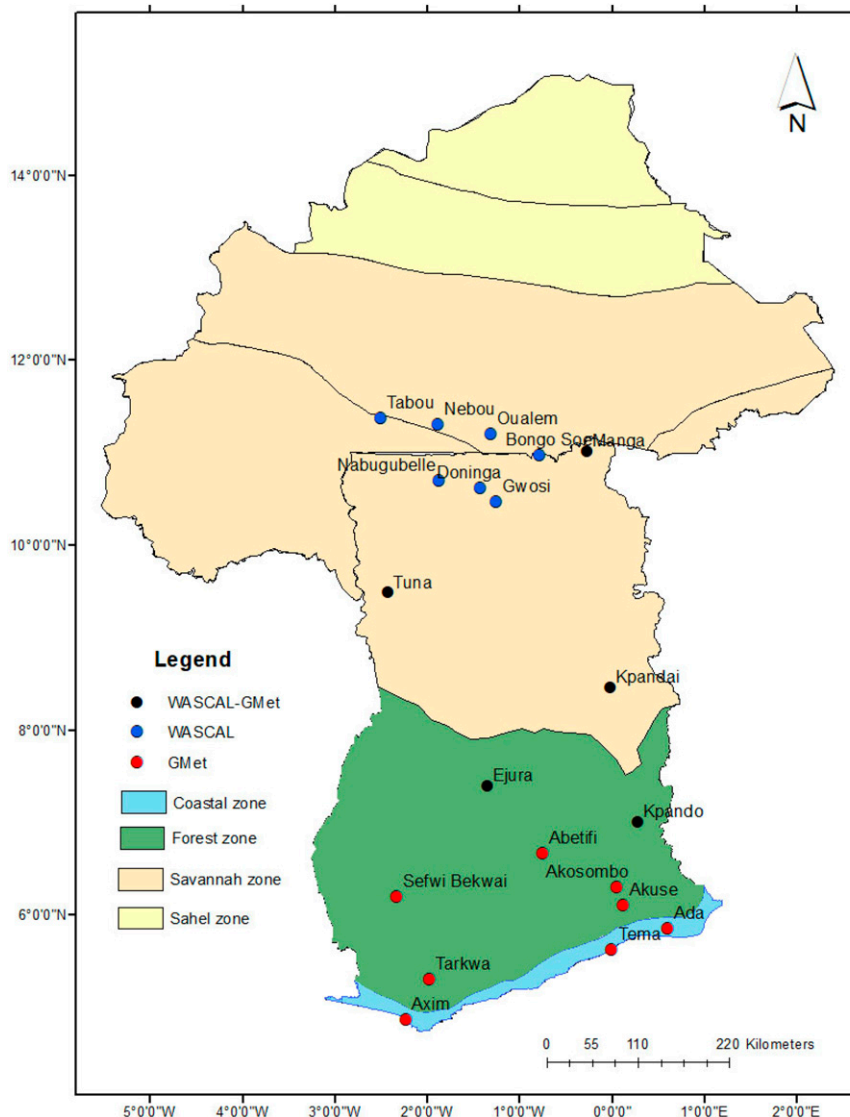
FIG. 2. Study area and location of the various AWSs used in this study. The red dots show the GMet AWSs, and the blue dots indicate the WASCAL AWSs. The black dots show the transnational climate observation network installed by WASCAL in Ghana. The different AWS networks have been established in recent years. The colored zones on the map show the different climate zones in the study area.

structure of the planetary boundary layer (PBL). For this study, the Mellor–Yamada–Nakanishi–Niino (MYNN) PBL scheme was chosen because it improves the representation of nonlocal mixing, subgrid-scale clouds, and turbulent interactions with clouds, and is also coupled with radiation schemes (Olson et al. 2019).

Five simulation experiments were performed with four different SW radiation schemes, namely, the Community Atmosphere Model (CAM), the modified Goddard (GoddardM), Dudhia, and the RRTMG in this study (Table 1). For the last SW scheme, another experiment coupled with aerosol inputs (RRTMG_AERO) was conducted. Each configuration used the same physical schemes as mentioned above but differed in terms

of LW radiation schemes. However, for the RRTMG_AERO experiment, we used the aerosol-aware Thompson microphysics scheme to account for the direct effect of aerosols (Thompson and Eidhammer 2014). To activate the effect of direct aerosol, we used the method of Ruiz-Arias et al. (2014), where we provided the AOD 550 nm and the Ångström exponent (AE) data from Copernicus Atmosphere Monitoring Service (CAMS) datasets. The CAMS data were also used as aerosol input for solar irradiance estimation in Spain with the WRF-Solar model (Sosa-Tinoco et al. 2022). The data from CAMS were bilinearly interpolated onto the grids of both domains. Moreover, the process of assimilating aerosol in the WRF-Solar model is similar to other climate models. Instead of

TABLE 1. Overview of the parameterization schemes used for the different WRF-Solar configurations. In total, five simulation experiments with different SW radiation schemes were performed, as listed; the RRTMG_AERO experiment takes into the account the effect on aerosols.

Physics	CAM	Dudhia	GoddardM	RRTMG	RRTMG_AERO
Radiation SW	CAM	Dudhia	Goddard	RRTMG	RRTMG + aerosols
Radiation LW	CAM	RRTMG	Goddard	RRTMG	RRTMG
Microphysics			Thompson		Aerosol-aware Thompson
Land surface			Noah land surface model		
Planetary boundary layer			MYNN		
Shallow cumulus			Deng cumulus		
FARMS			Activated		

being parameterized directly, the AOD is transferred through the radiative transfer routine for each simulated grid cell and updated 3-hourly. Each spectral band within the RRTMG scheme (from 0.2 to 12.2 μm) is parameterized based on the vertically integrated AOD and a reference aerosol type. Using reference aerosol types and relative humidity, the WRF Model calculates the aerosol single scattering albedo (SSA) and aerosol asymmetry parameters (ASY; Ruiz-Arias et al. 2014). The simulation period is from 1 December 2018 to 31 December 2019, and the entire month of December 2018 was used for the spinup. The GHI from the simulations is given in hourly instantaneous values.

c. Data

1) STUDY AREA

This study uses ground measurement data in Ghana and some parts of Burkina Faso (Fig. 2) for comparison of model output. The observation networks are located in different climatic zones and can be classified into three main zones: the coastal, the forest, and the savannah zone (Bessah et al. 2022). The coastal and the forest zones are characterized by a mean annual rainfall of between 1000 and 1600 mm within 7–10 months, while the savannah zone receives a mean annual rainfall between 700 and 1200 mm within 5–7 months (Bliefernicht et al. 2019, 2018; Nicholson 1981). The savannah region is also characterized by a pronounced dry season (from November to April), whereas the coastal and forest zones are characterized by a much longer rainy season and a bimodal rainfall regime, especially along the coast. In the coastal and forest zones, total cloud cover can be up to 50% in the dry season and about 80%–100% in the wet season. In the savannah area, total cloud cover is much lower in the dry season (25%–30%) and higher in the rainy season (70%–80%; Nicholson et al. 2018). Additionally, the region experiences aerosol particles from the Saharan desert and also from biomass burning during the December–February season, also called the Harmattan period.

2) GROUND DATA

We used GHI data collected from two different meteorological networks established by WASCAL and partner institutions in this region (Fig. 2; Salack et al. 2019; Bliefernicht et al. 2018). In addition, GHI data collected from an AWS network operated by GMet were used. The different AWSs are handled and maintained by WASCAL and GMet. The Tabou, Nebou, Oualem, Nabugubelle, Doninga, and Gwosi stations are part of the meteorological network operated under the WASCAL hydrometeorological observatory established in this region from 2012 to 2014 (Bliefernicht et al. 2018), whereas the remaining WASCAL stations (Manga, Kpandai, Ejura, and Kpando) belong to a new transnational climate observation network that was set up in 10 West African countries starting from December 2017 (Salack et al. 2019). GMet's AWS network was established in 2018. The solar radiation sensors are usually cleaned and checked twice a month to avoid dust accumulation. However, this cannot be guaranteed for all sites and periods as many sites are not permanently manned and some of them are located in remote areas, and because of other constraints. Moreover, fieldwork is organized on different sites to recalibrate or replace the sensors if they are defective. More details on the data collected by WASCAL's meteorological networks and the quality assurances applied can be found in Salack et al. (2019) and in Bliefernicht et al. (2018). Because of the different AWS networks, GHI is recorded at different time steps (5, 10, and 15 min) at different locations (see Table 2). GHI data used in this study were measured at 20 locations from AWSs (Fig. 2). The study area includes three stations from the southern part of Burkina Faso and 17 stations from Ghana distributed throughout the country.

For this study, hourly instantaneous values of GHI were considered to match the WRF output simulation with a time slice from 1 January 2019 to 31 December 2019. Missing hourly instantaneous values of GHI are replaced by the interpolated value of GHI within the 30 min, assuming that the value of GHI does not deviate significantly during this period. However, data gap filling was only performed for small data gaps by performing a temporal infilling using the nearest observations, assuming that the value of GHI does not differ significantly within this period. For larger data gaps, no infilling was performed. The number of missing values in Table 2 shows that most time series are complete. Thus, we assume that the current applied infilling techniques had only a minor impact on the model performance. According to Batista and Monard (2003), a ratio of missing values of less than 1% has no impact on the applied performance measures, while a ratio of more than 5% requires the application of a data gap filling technique.

TABLE 2. List of the AWSs with their number of missing data, time resolution, and their source and the average solar radiation for the study period (1 Jan–31 Dec 2019). The value in the parentheses of the column of the number of missing values indicates the ratio of missing values of different AWSs.

Station	No. of missing values	Institution	Time resolution (min)	Avg mean (W m^{-2})
Bongo Soe	4 (0.05%)	WASCAL	5	153.61
Doninga	258 (2.95%)			207.54
Gwosi	0 (0.00%)			215.32
Nabugubelle	0 (0.00%)			217.4
Nebou	0 (0.00%)			228.55
Oualem	1 (0.01%)			218.45
Tabou	740 (8.45%)			213.72
Ejura	385 (4.39%)	WASCAL–GMet	10	186.32
Kpandai	0 (0.00%)			181.21
Kpando	329 (3.76%)			180.78
Manga	0 (0.00%)			214.57
Tuna	364 (4.16%)			198.82
Abetifi	0 (0.00%)	GMet	15	195.93
Ada	0 (0.00%)			204.17
Akosombo	0 (0.00%)			193.83
Akuse	0 (0.00%)			184.85
Axim	0 (0.00%)			184.85
Sefwi Bekwai	0 (0.00%)			173.87
Tarkwa	0 (0.00%)			153.1
Tema	0 (0.00%)			198.82

In this study, no data gaps were filled to maintain the integrity of the data for better model evaluation.

3) ERA5 REANALYSIS DATA

ERA5 is the fifth-generation of ECMWF reanalysis data with a horizontal grid spacing of ~31 km and 37 pressure levels from 1000 (surface) to 1 hPa (Hersbach et al. 2020); it has superseded ERA-Interim reanalysis data. ERA5 is built on a 4D-Var data assimilation using cycle 41r2 of the Integrated Forecasting System (IFS). It covers the period from 1950 to the present. The ERA5 reanalysis data are widely used for climate and related studies (Xia et al. 2022; Dommo et al. 2022; Adeniyi 2020). We retrieved hourly surface and atmospheric pressure data from 1 December 2018 to 31 December 2019 for ILBC of the WRF-Solar model.

4) CAMS DATASETS

All the AOD 550 nm and AE data used in this study are from the CAMS near-real-time global analysis and forecast model. CAMS is operated by ECMWF, and over 60 satellites are used to combine atmospheric composition information with state-of-the-art atmospheric models to produce quality-controlled information and data (Peuch et al. 2018; Flemming et al. 2015). CAMS has a spatial resolution of about 40 km, with 137 levels from the surface up to 0.1 hPa. We retrieved 3-hourly total AOD at 469, 550, and 865 nm within a time ranging from 1 December 2018 to 31 December 2019. Since CAMS does not provide AE data, AE is estimated from the measurement of the optical thickness of an AOD layer at two different wavelengths (we used AOD 469 and AOD 865 nm) using the equation of Schuster et al. (2006):

$$AE = -\frac{\log\frac{\tau_{\lambda_1}}{\tau_{\lambda_2}}}{\log\frac{\lambda_1}{\lambda_2}}, \tag{1}$$

where τ_{λ_1} and τ_{λ_2} are the total AOD at wavelength λ_1 and λ_2, respectively.

d. Methods

1) MODEL EVALUATION

The evaluation of the different experiments is achieved by comparing the hourly instantaneous GHI values from the WRF-Solar model and the in situ data. A nearest-neighbor interpolation method is applied to extract the different locations in the simulation results that correspond to the same geographical coordinates of the station. For the performance of the different simulations versus observations, we consider GHI from the observation when the solar zenith angle (SZA) is <80° to avoid early-morning and late-evening errors in GHI due to measurement uncertainties (Flemming et al. 2015) and also the seasonal effects of sunset and sunrise. In the region, SZA < 80° corresponds to an average of 0800 to 1700 UTC; the diurnal variation of GHI is analyzed in this time window. We performed three types of analyses: all-sky conditions, cloudy conditions, and clear-sky conditions. In the case of all-sky conditions, the entire observational data are used for the model comparison. In the second and third analyses, the observational data are grouped into different categories based on the clearness index (Kt) to determine cloudy and clear-sky day composite. Kt is defined as the ratio of the global solar irradiance measured at

ground-level GHI to the top of the atmosphere extraterrestrial radiation (G_0):

$$Kt = GHI/G_0. \tag{2}$$

The daily extraterrestrial radiation G_0 (MJ m^{-2} day^{-1}) is obtained using the following equation (Allen et al. 1998):

$$G_0 = \frac{24(60)}{\pi} G_{SC} d_r [\omega_s \sin(\varphi) \sin(\delta) + \cos(\varphi) \cos(\delta) \sin(\omega_s)], \tag{3}$$

where G_{SC} is the solar constant (=0.0820 MJ m^{-2} min^{-1}), d_r is the inverse relative distance for Earth–Sun (rad), ω_s is the sunset hour angle (rad), φ is the latitude of the location (rad), and δ is the solar declination (rad).

The values of the clearness index used to define cloudy and clear skies vary according to location. Cloudy and clear-sky conditions are given when $0.12 \leq Kt < 0.35$ and $Kt \geq 0.6$, respectively, following other studies done in West Africa (Okogbue et al. 2009; Kuye and Jagtap 1992). The daily mean GHI is computed by averaging the instantaneous GHI when there are no missing values of GHI within a day. In addition, an algorithm is used to find all days that fall under the criteria of "cloudy sky" and "clear sky" for different AWS sites, and for each class, an average diurnal cycle of GHI is computed. Independently from the observations, the same calculations are done for the simulated data to obtain the different sky conditions for five WRF-Solar experiments at different locations.

2) QUALITY CONTROL OF THE OBSERVATION DATA

The main purpose of the quality control of the observations within this study is to remove all samples that are outside the normal range of GHI. This is done using the physically possible limit [Eq. (4)] and the extremely rare limit [Eq. (5)] of GHI from the guidelines of the Baseline Surface Radiation Network (BSRN; BSRN 2021) as follows:

$$-4 \text{ W m}^{-2} < GHI < I_0 1.5 \cos \cos(SZA)^{1.2}$$
$$+ 100 \text{ W m}^{-2} \quad \text{and} \tag{4}$$

$$-2 \text{ W m}^{-2} < GHI < I_0 1.5 \cos \cos(SZA)^{1.2} + 50 \text{ W m}^{-2}, \tag{5}$$

where I_0 the solar constant. After the evaluation of the 20 stations, 1473 measurement values were flagged by the BSRN limits. However, some samples passed the test even though the sensor on site always measured low GHI due to calibration or defective sensors. For this reason, a second quality control was performed by computing the daily clearness index. If the number of clear-sky conditions (Ncs; $Kt \geq 0.6$) for a year was not appropriate, we discarded the station. At the end of this scan, Bongo Soe (Ncs = 0) from the WASCAL network and Tarkwa (Ncs = 6) from the GMet network were removed from the AWS network for further analysis.

3) PERFORMANCE MEASURES

The performance of the WRF-Solar model is evaluated in terms of different measures to address specific performance attributes like skill and accuracy (Wilks 2011). To estimate the average accuracy of the WRF simulations, we used the mean absolute error (MAE):

$$MAE = \frac{1}{n} \sum_{i=1}^{n} (|P_i - O_i|), \tag{6}$$

and its normalized measure (nMAE):

$$nMAE = \left[\frac{MAE}{\max(O) - \min(O)} \right] \times 100, \tag{7}$$

where P_i is the simulation value, O_i is the observation data at time step I, and n is the number of data points used for comparison; $\max(O)$ and $\min(O)$ are the maximum and minimum value of the observations. In addition, further accuracy measures are computed, namely, the root-mean-square error (RMSE):

$$RMSE = \sqrt{\sum_{i=1}^{n} \frac{(P_i - O_i)^2}{n}}, \tag{8}$$

and the normalized RMSE (nRMSE):

$$nRMSE = \left[\frac{RMSE}{\max(O) - \min(O)} \right] \times 100. \tag{9}$$

Like the mean-square error (MSE), the RMSE and MAE are two of the most frequently used scores for evaluation of numerical simulations and predictions (Neill and Hashemi 2018). Since the calculation of the MAE is based on absolute deviations, the MAE is a more robust measure compared with MSE. Moreover, in the case of RMSE and MAE, the physical units remain the same as the target variable for the model comparison, which is watts per meter squared for this study. Thus, the interpretations of the error values of the MAE and RMSE are much easier compared with the MSE.

In addition, the degree of linear dependence between simulation and observation is measured by computing the Pearson's correlation as follows:

$$R = \frac{\sum_{i=1}^{n} (O_i - \underline{O})(P_i - \underline{P})}{\sqrt{\sum_{i=1}^{n} (O_i - \underline{O})^2 \sum_{i=1}^{n} (P_i - \underline{P})^2}}, \tag{10}$$

where $\underline{O}$ and $\underline{P}$ are the mean value of the observation and simulation, respectively. We also computed the index of agreement (IOA) to assess the performance of the WRF-Solar output (Legates and McCabe 2013):

$$IOA = 1 - \frac{\sum_{i=1}^{n} (P_i - O_i)}{\sum_{i=1}^{n} (|P_i - \underline{O}||O_i - \underline{O}|)^2}. \tag{11}$$
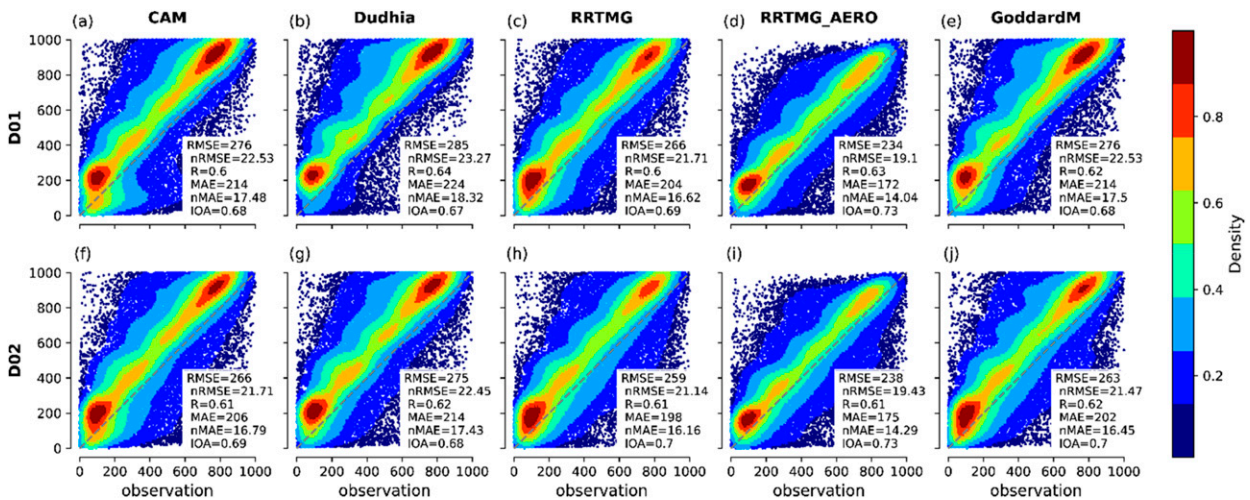
FIG. 3. Density plot of hourly values of GHI from different WRF-Solar simulations and domains (W m^{-2}) vs observation for 18 stations (W m^{-2}) using Gaussian kernels with values normalized to 0–1. The dashed gray line exhibits the 1:1 line. RMSE (W m^{-2}), R, IOA, and MAE (W m^{-2}) indicate the root-mean-square error, the Pearson's correlation, the index of agreement, and the mean bias error, respectively, and the nRMSE (%) and nMAE (%) indicate the normalized root-mean-square error and the normalized mean bias error, respectively.

In contrast to the aforementioned performance measures, R and IOA are both skill scores and are therefore comparing the quality of the WRF-Solar simulations against a low-skill reference simulation.

3. Results and discussion

Assessment of WRF-Solar simulations

1) SCATTERPLOT

Most simulations show a good estimate of GHI for the 18 stations for the all-sky conditions (Fig. 3). The scatterplots show two major clusters, around 200 and 800 W m^{-2}. Moreover, the scatterplots are not symmetrical, and the major core values are on the left side of the diagonal (line: 1:1 line). In other words, the simulations tend to overestimate the observed values of GHI. The inner domains perform slightly better than the outer domains in terms of RMSE, MAE, R, and IOA irrespective of their simulation, except for RRTMG_AERO, where domain D1 performs better than domain D2. For instance, RRTMG_D01 indicates a value of RMSE of 266 W m^{-2} (21.71%), MAE = 204 W m^{-2} (16.62%), R = 0.6, and IOA = 0.69, whereas RRTMG_D02 has an RMSE value of 259 W m^{-2} (21.14%), MAE = 198 W m^{-2} (16.16%), R = 0.61, and IOA = 0.7. In general, the high resolution improves the estimation of GHI over the region. This is consistent with previous studies where the authors showed that high-resolution simulations improve the estimation of GHI using the WRF-Solar model (Sosa-Tinoco et al. 2022; Gueymard and Jimenez 2018).

Dudhia_D02 has the lowest performance, while RRTMG_AERO_D01 has the highest performance with the following values: RMSE: 234 W m^{-2} (19.1%); MAE: 172 W m^{-2} (14.04%); and IOA: 0.73. Our results are also comparable to

some results in other regions (Verbois et al. 2018; Zempila et al. 2016). For example, Verbois et al. (2018) found an RMSE of 242 W m^{-2} for hourly solar irradiance in day-ahead forecasting in Singapore with the WRF-Solar model. In addition, there is a large deviation of 20–30 W m^{-2} in terms of RMSE between RRTMG and RRTMG_AERO in both domains. This shows that the WRF-Solar model coupled with aerosol input improves the estimated GHI over the region because aerosol absorbs and scatters incoming solar beam. This was also highlighted by Jiménez et al. (2016b), who showed that including aerosol in the WRF-Solar simulation improves the estimate of GHI by 5%–28%.

Despite the good performance of RRTMG_AERO_D01, the high value of RMSE shows that the model is struggling to estimate the GHI over the study area. This could be due to the low amount of cumulus clouds in the model (Ruiz-Arias et al. 2016). In addition, the development of low-level clouds in West Africa, especially in the southern part, is still not well parameterized in climate models in terms of cloud amount and frequency (Hannak et al. 2017; Knippertz et al. 2011). Danso et al. (2020) have shown that the low-level clouds attenuate incoming solar radiation and about 49% and 44% is lost at the surface in the Guinea and Sahel, respectively. Another reason could also be related to the representation of aerosol–cloud–radiation feedback in the model, or biases in aerosol input (Cheng et al. 2022). The bias could also be related to the 3D radiative effect, which leads to overshooting of GHI, or too high values of the solar zenith angle generated by the model.

2) SPATIAL DISTRIBUTION

Figures 4 and 5 show the spatial nRMSE and nMAE values, respectively, in relation to the model performance at different stations. High nMAE and nRMSE values are located
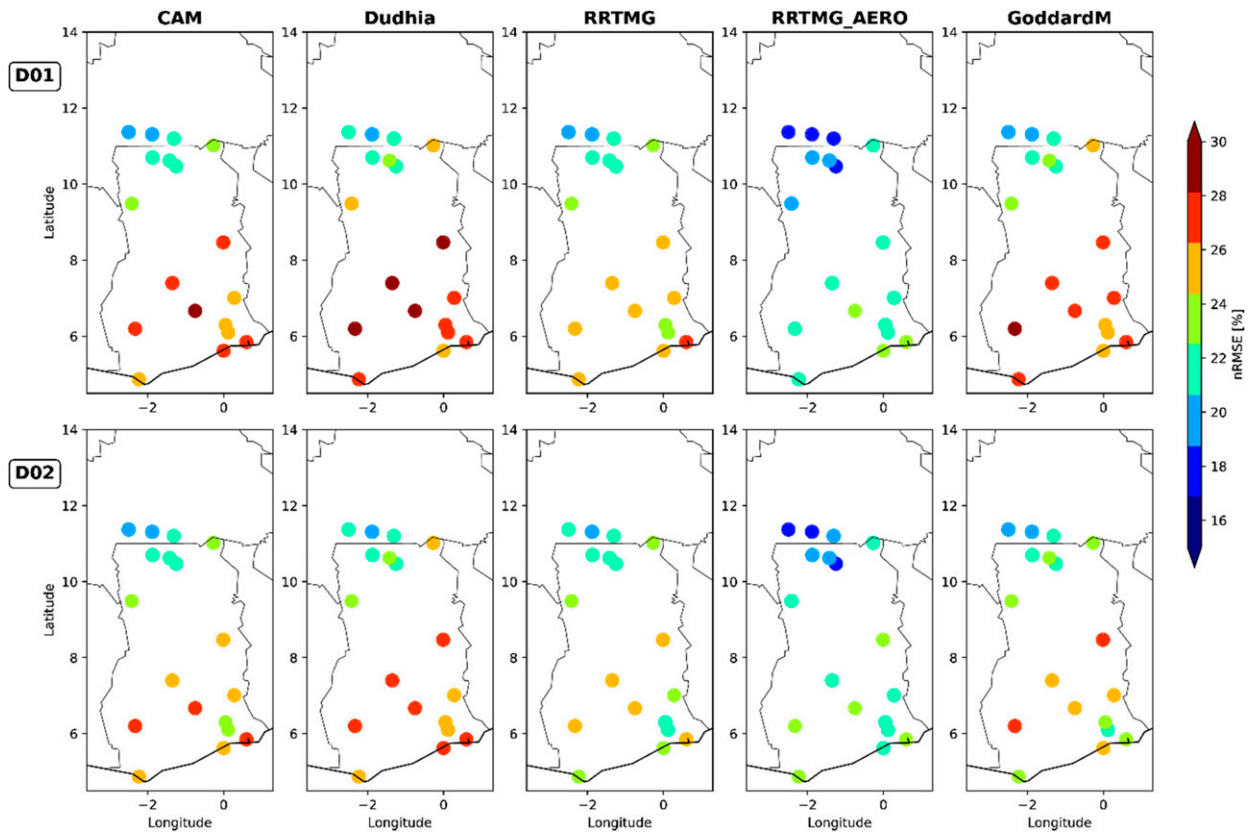
FIG. 4. Spatial distribution of the nRMSE of hourly solar irradiance over the studied domain. The first row represents the outer domain D1, and the second row represents the inner domain D2. Each column indicates the different experiments used in the WRF-Solar model.

in the southern part, while low nMAE and nRMSE values are found in the northern part. Additionally, the high resolution [inner domain (D2)] of the different simulations reduces the values of nRMSE and nMAE compared with their outer domain (D1), except for that of RRTMG_AERO. In general, RRTMG_AERO_D01 exhibits the lowest values of nRMSE and nMAE for all the stations. Our results suggest that the biases are lower in cloud-free areas (Savannah region) and higher in cloudy areas (Guinea region). The discrepancy between the two areas could be attributed to the shallow cumulus parameterization and/or cloud properties in the WRF-Solar model. Pedruzo-Bagazgoitia et al. (2019) have shown that the shallow cumulus parameterization used in the WRF-Solar model (Deng et al. 2014) has difficulty reproducing the main features that clouds exert on the surface–atmosphere system because the scheme produces clouds that are too dense, cloud bases that too high, and abrupt formation of a second cloud layer that is too high. In addition, the timing of the started shallow updrafts to the transition to deep convection could be missed by the shallow convection scheme in the region. These could also have an effect on the absorption, scattering, or reflection of the incoming SW radiation by the clouds. The shallow convection parameterization has been acknowledged as one of the main challenges among NWP models, even at a high-resolution scale (Hong and Dudhia 2012).

3) SEASONAL PERFORMANCE

The seasonal performance of WRF-Solar GHI with respect to ground measurements is displayed in Fig. 6. Most simulations exhibit high median values of nRMSE during the June–August (JJA) season (rainy season), which are typically associated with considerable high nMAE. Both metrics are similar but differ in terms of magnitude. This is in line with the findings of Sawadogo et al. (2022), who showed that a high deviation of the hourly estimated GHI occurred during the JJA season. The large deviation could be related to the increase in relative humidity, which, in turn, leads to high cloud cover and frequent thunderstorm activities, aerosol loads, and deep and shallow convection during the rainy season (Akinsanola and Ogunjobi 2017; Sylla et al. 2016). Moreover, the high median values of nRMSE and nMAE observed in this study could also be explained by 3D cloud effects, cloud inhomogeneities, or optical properties of the clouds, which are not reproduced in detail in the WRF-Solar model during the rainy season. The RRTMG_AERO followed by the RRTMG experiment indicates the best performance in the JJA season. The SON season also shows high median nRMSE and nMAE of most simulations with high variability. The high variability is due to the fact that the northern and southern parts of the studied area lag behind the rain by one and/or two months. Low values of nRMSE and nMAE occur in the DJF season,
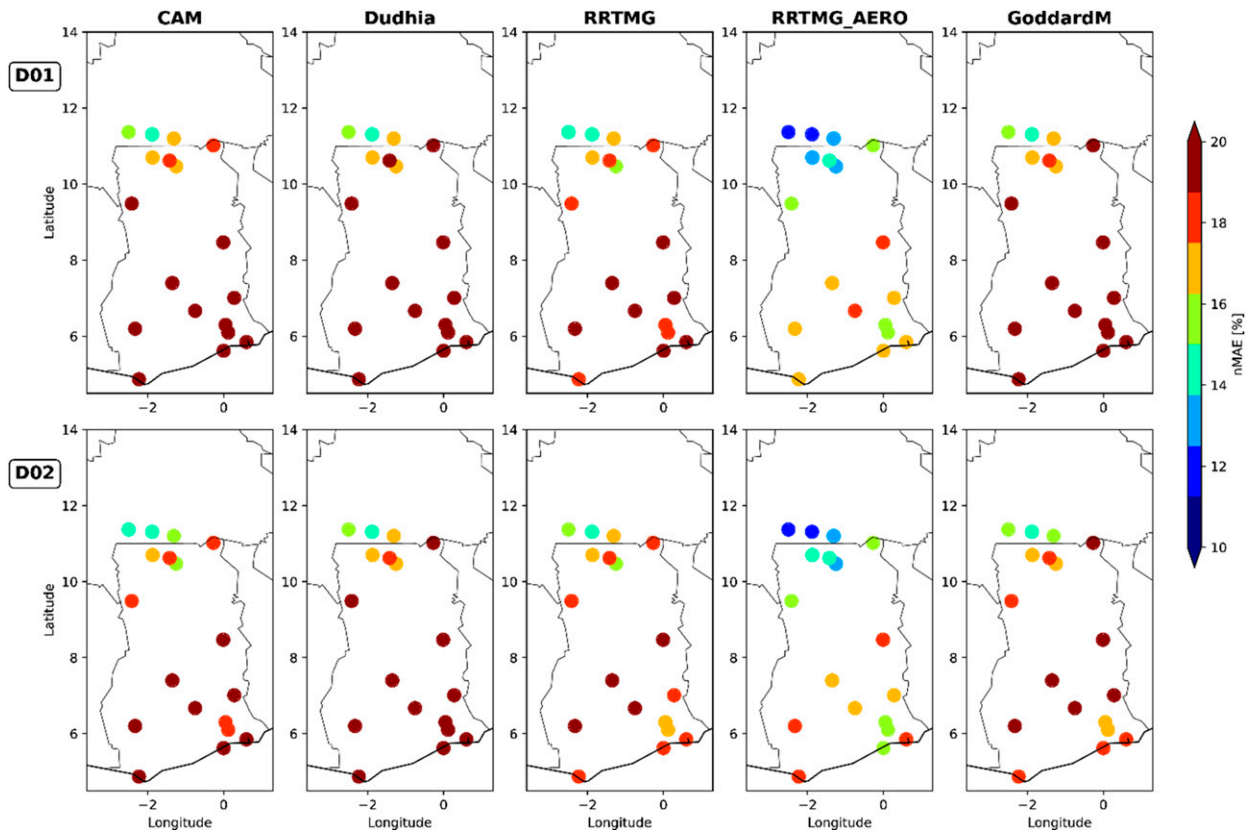
FIG. 5. As in Fig. 4, but for the nMAE.

with a high variability. The low nRMSE and nMAE could be due to the cloudless conditions in the region. RRTMG_AERO shows a large improvement over the other simulations of about 5%–10% in terms of nMAE. This result shows that considering time-varying aerosol in the RRTMG SW radiation scheme of WRF-Solar can improve the simulation of GHI even during the Harmattan period in the region. Overall, the RRTMG_AERO experiment shows the best performance in all seasons.

4) DIURNAL VARIATION

For the diurnal cycle, three AWSs with no missing values are chosen for comparison with WRF-Solar. The three AWSs are in the three climate zones of the study area: Ada (coastal zone), Akosombo (forest zone), and Nebou (savannah zone).

(i) All sky

The average diurnal pattern of GHI varies for different locations under all-sky conditions (Fig. 7). Most simulations fall within the 95% confidence interval of the measurement for the three climate zones. The minimum average value occurs in the coastal zone (Ada), while the maximum occurs in the savannah zone (Nebou), and the maximum of GHI occurs around noon when the solar zenith angle of the sun reaches its minimum. The average maximum value during this period of the observation is about 700 (Ada and Akosombo) and

750 (Nebou) W m^{-2}. Furthermore, the performance of different experiments depends on the climate zone. In the coastal zone, the experiments CAM_D01 and GoddardM_D01 are able to capture the peak of the observation. The simulations with aerosol input (RRTMG_AERO) underestimate the average diurnal variation of the observation and therefore miss capturing the peak of the diurnal variation with a large bias (RRTMG_AERO_D02). RRTMG_AERO also underestimates the peak of GHI in the forest zone (Akosombo), whereas RRTMG captures the peak of the GHI well. This bias could be a result of persistent stratiform low-level clouds in the early afternoon hours that have been formed during nighttime (Schrage and Fink 2012; Knippertz et al. 2011); the stratiform low-level clouds have a significant impact on the surface radiation in the southern part of West Africa (Hill et al. 2018). This suggests that the RRTMG_AERO simulations produce more clouds compared with reality or that the feedback between aerosol and clouds is not well represented along the coastal and forest zones. However, in the savannah zone (Nebou), RRTMG_AERO mimics the average diurnal cycle well and captures the peak of the GHI, whereas the other experiment shows an overestimation.

(ii) Cloudy sky

Figure 8 exhibits the average diurnal variation of GHI, which was determined for cloudy-days composite for different
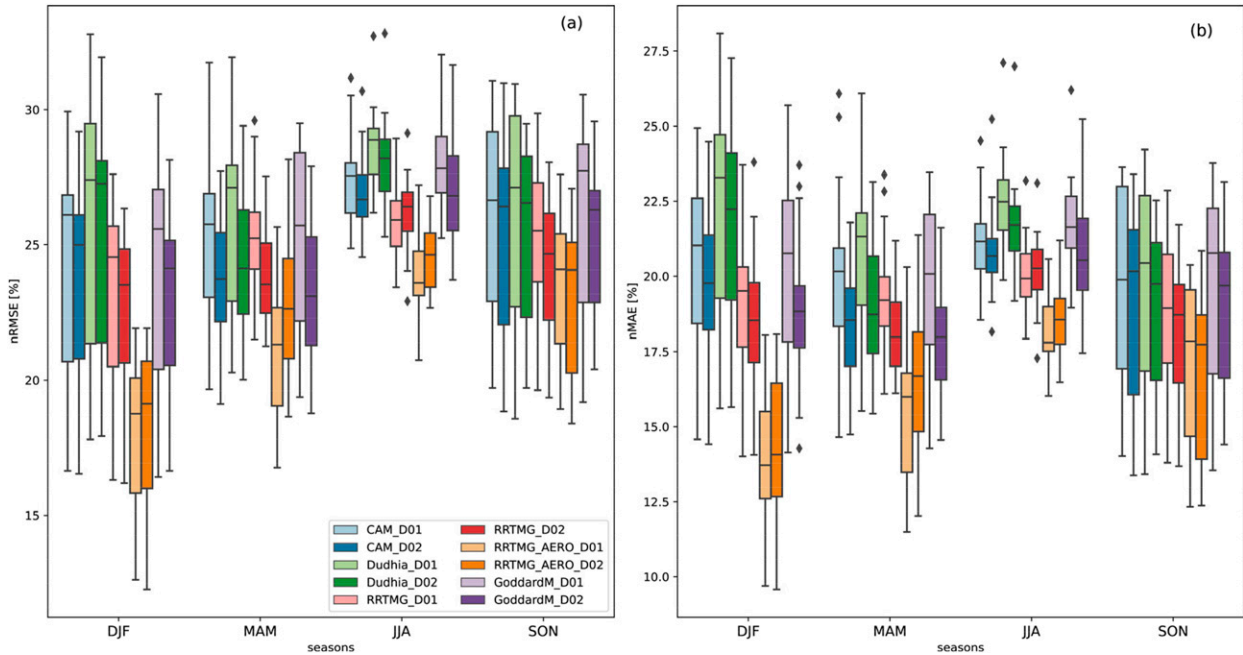
FIG. 6. Seasonal performance of simulated GHI for the different WRF-Solar configurations, showing the spread of the (a) nRMSE and (b) nMAE for the 18 stations.

stations. All experiments are not able to mimic well the pattern of diurnal variation of GHI. The number of days that occur under cloudy-days composite varies from station to station. Akosombo (located in the forest zone) indicates the highest number of days (59), while Nebou (northern part of the study) shows the lowest value (24). The performance of the different experiments differs for each station. All experiments show an overestimation of the daily course of GHI in all stations. For instance, while the maximum value of GHI of the observation is below 400 W m^{-2}, some experiments show a value of more than 600 W m^{-2}, especially in Nebou. This could be due to the fact that the WRF-Solar produces fewer

clouds than it should when the sky is cloudy. This leads to a similar conclusion to Gueymard and Jimenez's (2018) finding that the WRF-Solar model is not able to reproduce cloud-enhanced situations. However, RRTMG_AERO shows less bias in the diurnal average variation of GHI in Akosombo and Nebou. A similar result was obtained in Shagaya, Kuwait, where WRF-Solar, configured with an RRTMG SW radiation scheme forced with aerosols failed to capture the observed GHI under cloudy-day conditions (Gueymard and Jimenez 2018). This could be related to the feedback from aerosols and clouds, which could be a factor explaining the discrepancies between RRTMG_AREO and the observations. The
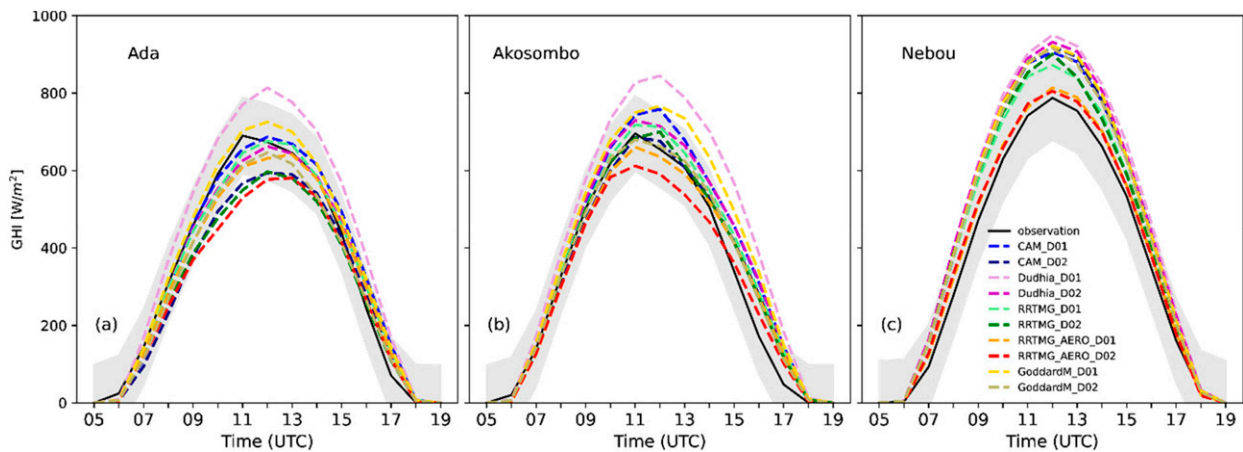

FIG. 7. Annual average diurnal variation of WRF-Solar simulations and observation of the GHI at different stations for 2019. The gray shaded curve indicates the 95% confidence interval of the measurement.
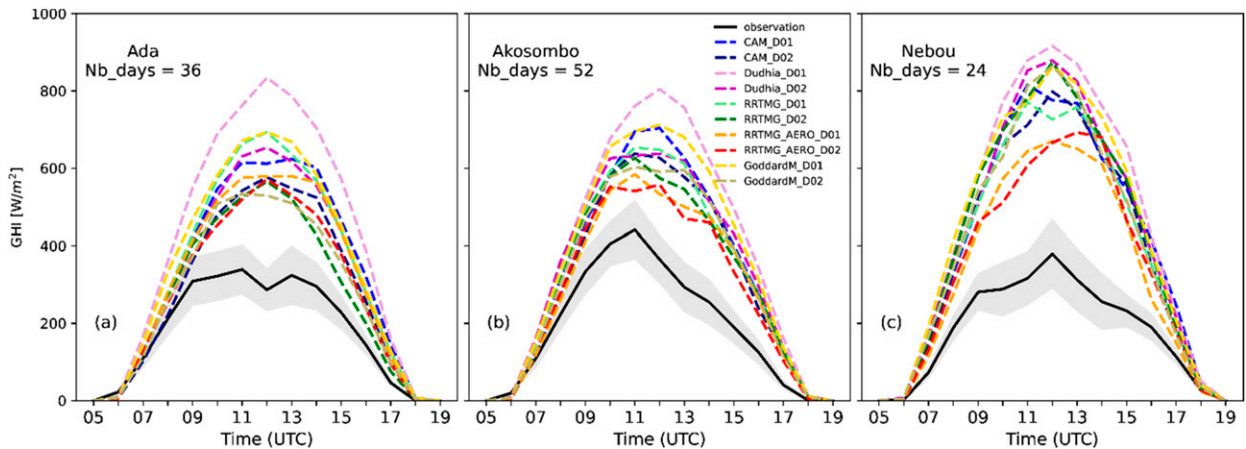
FIG. 8. Average diurnal variation of different WRF-Solar configurations and observation of the GHI at different stations under cloudy conditions. The Nb_days indicates the number of times that a cloudy day occurs.

temporal resolution does not allow us to simulate a small variability of clouds, which could also be a factor for the biases on cloudy days. This region is known as a challenging region in terms of weather, and climate models fail to accurately depict the low- and middle-level cloudiness, where these types of clouds are abundant and frequent (Hannak et al. 2017). Moreover, the bias could be also related to the fact that the clouds produced in the model do not appear at the right place at the right time. In summary, the interaction between clouds and aerosols over the West Africa region needs to be improved. The shallow cumulus parameterization also needs to be improved to enhance the representation of clouds in the model.

(iii) Clear sky

Under clear-sky day composites, the performance of the WRF-Solar simulations also varies at the different sites (Fig. 9). Most simulations are able to capture the average diurnal variation of the GHI with notable biases. The performance of the different experiments also differs between the southern and northern parts of the study area. More clear-sky day composites

(183) are in the northern part than in the southern part. In the southern part (coastal and forest zones), all the experiments underestimate the daily course of GHI, while in the northern part, some of them overestimate the values of GHI. RRTMG_AERO captures well the observed average diurnal variation of the GHI in Nebou; they even partially overlap. The good performance of RRTMG_AERO in Nebou could be due to a good interaction between aerosol and radiation. This suggests that including the direct effect of aerosol in the WRF-Solar model could better reflect the diurnal variation of GHI in cloud-free areas. However, in the southern part, RRTMG_AERO does not perform well, whereas Dudhia_D01 shows the best pattern compared with other simulations. The poor performance of the different experiments in the southern part could be related to the fact that fewer days with clear-sky conditions are produced in the simulations than in reality, while in the northern part, some simulations produce more clear-sky days. The poor performance of RRTMG_AERO in Figs. 9a and 9b can also be attributed to two factors: a bias of the aerosol data from CAMS and/or the type of aerosol simulated. Regarding the first factor, CAMS can introduce a bias
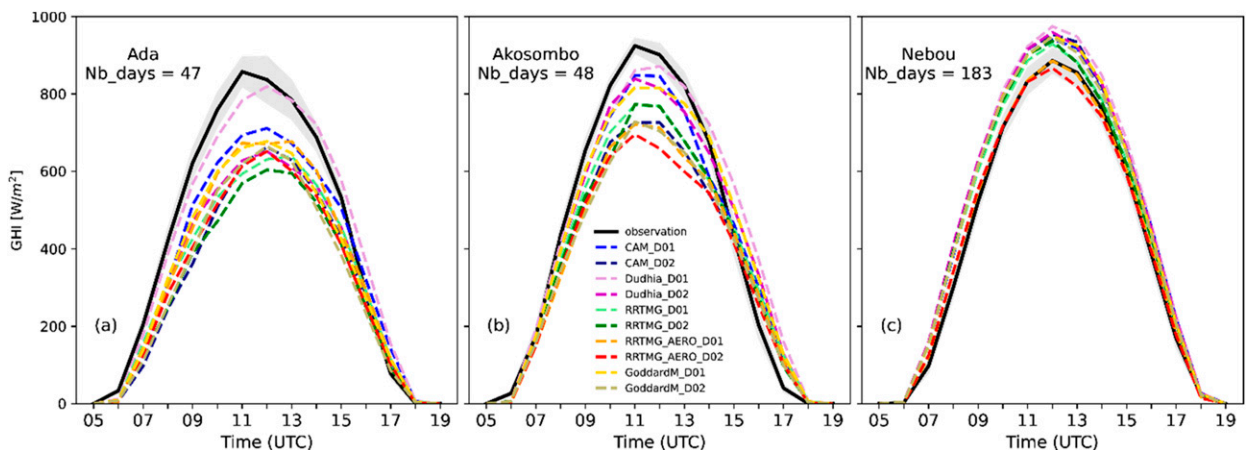

FIG. 9. As in Fig. 8, but under clear-sky conditions.

TABLE 3. Error metrics of different WRF-Solar experiments and atmospheric conditions on the GHI of the aggregated 18 stations.

			D1					D2		
	CAM	Dudhia	RRTMG	RRTMG_AERO	GoddardM	CAM	Dudhia	RRTMG	RRTMG_AERO	GoddardM
					Cloudy sky					
RMSE	359	411	351	303	390	348	374	346	305	357
nRMSE	33.33	38.16	32.13	28.13	36.21	32.31	34.73	32.13	28.32	33.15
R	0.37	0.40	0.38	0.37	0.39	0.36	0.39	0.38	0.38	0.40
MAE	284	340	275	239	3145	273	298	269	237	280
nMAE	26.38	31.59	25.57	22.15	29.22	25.27	27.71	24.95	22.04	26.03
IOA	0.46	0.42	0.47	0.52	0.44	0.47	0.45	0.47	0.52	0.46
					Clear sky					
RMSE	200	176	205	183	184	192	188	199	195	191
nRMSE	17.24	15.17	17.67	15.78	15.86	16.55	16.21	17.16	16.81	16.47
R	0.75	0.82	0.73	0.76	0.78	0.76	0.78	0.74	0.74	0.76
MAE	147	134	148	122	138	143	141	147	130	143
nMAE	12.64	11.59	12.73	10.50	11.90	12.30	12.18	12.28	11.23	12.37
IOA	0.77	0.81	0.76	0.79	0.79	0.78	0.79	0.77	0.77	0.78
					All sky					
RMSE	276	285	266	234	276	266	275	259	238	263
nRMSE	22.53	23.27	21.71	19.10	22.53	21.71	22.45	21.14	19.43	21.47
R	0.60	0.64	0.60	0.63	0.62	0.61	0.62	0.61	0.61	0.62
MAE	214	224	204	172	214	206	214	182	175	202
nMAE	17.48	18.32	16.62	14.04	17.50	16.79	17.43	16.16	14.29	16.45
IOA	0.68	0.67	0.69	0.73	0.68	0.69	0.68	0.70	0.73	0.70

into the AOD retrieval due to a lack of clear-sky conditions in cloudy areas (Flamant et al. 2018). For instance, a bias in the AOD of CAMS was observed throughout the year in comparison with AERONET data in southern Ghana (Koforidua) (figure not shown). This is consistent with Léon et al. (2021), who also showed a bias of AOD data in the forest zone in Ghana. The second factor could be related to high levels of aerosols in the coastal and forest zones, where biomass burning is the main source of aerosols during the dry season (Flamant et al. 2018). The increased AOD levels lead to greater absorption of GHI. This is consistent with the finding of Liu et al. (2022) that high AOD loading in the model can reduce GHI due to enhanced aerosol scattering effects. The underestimation of diurnal cycle of the RRTMG_AERO suggests that it is necessary to improve the feedback between aerosol and radiation under clear skies, especially when the radiative transfer routine experiences high AOD loading.

Table 3 highlights the error metrics of different simulations for the whole of 2019, aggregated for the 18 stations under clear-sky, cloudy, and all-sky conditions. Most simulations perform better under clear skies than under cloudy skies. Take the example of the Dudhia_D01 experiment, where IOA = 0.81, R = 0.82, RMSE = 176 W m^{-2} (15.17%), and MAE = 134 W m^{-2} (11.59%) in clear sky, and these values are tied to IOA = 0.42, R = 0.40, RMSE = 411 W m^{-2} (38.16%), and MAE = 340 W m^{-2} (31.59%) in cloudy sky. Our results are consistent with previous studies in which the WRF or WRF-Solar model performs well in clear-sky conditions (Gueymard and Jimenez 2018; Gamarro et al. 2019; Kim et al. 2017). Our study suggests that RRTMG_AERO performs better in terms of RMSE and MAE compared with other simulations when simulating GHI under cloudy and

all-sky atmospheric conditions over the studied domain. Under clear skies, RRTMG_AERO and the Dudhia experiment show the best performance; however, RRTMG_AERO performs best with respect to MAE. The poor performance of Dudhia in all-sky condtions is related to its performance under cloudy skies. The inclusion of aerosol in the RRTMG experiment improves the performance in simulating GHI under all atmospheric conditions, which is in line with the results of Ruiz-Arias et al. (2013). Despite the good performance of RRTMG_AERO, the discrepancy with observations in terms of RMSE and MAE remains high. This could be attributed either to the bias of the input aerosol (Inness et al. 2019) or to the scheme used to simulate aerosol dynamics in terms of scattering and absorption of the incoming solar radiation in the WRF-Solar model, which is not suitable for this domain.

The accuracy of estimating GHI using the WRF-Solar model is affected by large compensating biases on clear and cloudy days. During cloudy-sky conditions, the GHI is strongly overestimated, while a low underestimation occurs during clear-sky conditions. The compensating biases arise from the inability of the model to accurately simulate clouds and aerosols. To enhance the accuracy of the GHI simulations using WRF-Solar, it is crucial to improve the parameterization of the Deng shallow convection scheme for the West Africa region. The assimilation of AOD in the radiative transfer model should be improved to reduce the biases of the GHI estimation under clear skies. This can lead to more accurate and reliable GHI, which is essential for solar energy application. Additionally, the underestimation of fractional cloud cover in deterministic model runs can result in a high bias of GHI under cloudy skies, as suggested by Ruiz-Arias et al. (2016) and Lara-Fanego et al. (2012). However, when

relying on a single model run to estimate GHI, any uncertainties can be not quantified. To solve this problem, an ensemble approach can be used to quantify uncertainties and to provide a more robust GHI estimation than a single deterministic model run. This approach is particularly useful for operators of solar power plants to quantify GHI uncertainties in the planning and management of electricity generation.

4. Summary and conclusions

In this study, the sensitivity of four SW radiation schemes (CAM, Dudhia, RRTMG, and New Goddard SW schemes) of the WRF-Solar model was investigated for the first time focusing on Ghana and southern Burkina Faso. The WRF-solar simulations were done for 2019 using two 1-way nested domains, where the outer domain had a spatial resolution of 15 km, and the inner domain had a resolution of 3 km. For the RRTMG scheme, we carried out two different experiments: one without providing aerosol information and one with aerosol inputs (RRTMG_AERO). For the model comparison, we used observed GHI in hourly resolution from 18 novel automatic weather stations from different networks established over the past years by WASCAL and GMet in this region. The stations' data were quality controlled using rigorous methods and criteria to identify and remove suspicious data. The evaluation of the WRF-Solar with the 18 stations was done for different weather conditions (all sky, clear sky, and cloudy) and different climatological regions (i.e., Guinean zone and Sudan savannah). The results of the study can be summarized as follows:

- The quality control of the observations showed that both data sources are quite good for evaluating the WRF-Solar model.
- Most simulations provide a relatively good estimation of the GHI observations for the 18 stations under all-sky conditions, with the general outcome that the RRTMG_AERO performs best.
- There is a clear north–south gradient of the model performance visible for all schemes, with lower model accuracies in terms of nRMSE and nMAE in the southern part (Guinean zone).
- The evaluation of the WRF solar simulations for different seasons leads to similar performance tendencies for the different radiation schemes. Lower values of nRMSE and nMAE occur during the DJF season, while higher nRMSE and nMAE values are obtained for the JJA season. The RRTMG_AERO experiment generally performs best for the different seasons.
- Most simulations mimic well the average diurnal variation of the observation at the different stations under all-sky conditions. The RRTMG_AERO reduces the biases under all-sky conditions, especially in the northern part.

In summary, the study showed that the WRF-Solar model coupled with aerosol input and the RRTMG SW scheme improves the simulation of GHI over the region. Despite the good performance of RRTMG_AERO under different sky conditions, the biases of the model are still high. It is therefore challenging for the model to simulate GHI under these conditions for the West Africa region. Consequently, further adaptation and model development of WRF-Solar is needed for this region, such as a further advancement of the parameterization schemes for deep and shallow convection to better simulate local unresolved clouds. In addition, future studies should focus on the improvement of feedback mechanisms between aerosol and clouds at a subgrid scale. Following the results of the study, direct normal irradiance (DNI) could also be evaluated and the forecast of GHI for 2–3 days ahead over the West African region could be investigated. Another study could also assess the GHI of WRF-Solar in convection-permitting simulation and the Deng shallow cumulus scheme at high resolution in the region. Given the uncertainties in estimating GHI, the use of the WRF-Solar ensemble prediction system (EPS) model could bring significant benefits to the region. To evaluate the performance gain of WRF-Solar EPS, a comparison of the two models (WRF-Solar and WRF-Solar EPS) needs to be done in future investigations. Moreover, the robustness of the configuration needs to be addressed in future studies. Despite these challenges, the results of this study provide an important benchmark for finding a suitable WRF-Solar model configuration for solar energy forecasts in West Africa. The current study provides important insight into the quality of WRF-Solar simulations and shows how suitable SW radiation schemes are for West Africa for solar energy applications like GHI forecasting and long-term GHI reconstruction.

Data availability statement. Automatic weather station data collected by WASCAL and GMet are not publicly available, and we do not have the right to share it with third parties. Data requests can be sent to WASCAL and GMet via the following email addresses: secretariat_cc@wascal.org and client@meteo.gov.gh. ECMWF data are freely available online [https://climate.copernicus.eu/climate-reanalysis (ERA5); https://apps.ecmwf.int/datasets/data/cams-nrealtime (CAMS)].

REFERENCES

Adeniyi, M. O., 2020: Simulating the influence of doubled CO_2 on the water budget over West Africa using RegCM4.7. *Meteor. Hydrol. Water Manage.*, **8**, 12–19, https://doi.org/10.26491/mhwm/125198.

Akinsanola, A. A., and K. O. Ogunjobi, 2017: Evaluation of present-day rainfall simulations over West Africa in CORDEX regional climate models. *Environ. Earth Sci.*, **76**, 366, https://doi.org/10.1007/s12665-017-6691-9.

Allen, R. G., L. S. Pereira, D. Raes, and M. Smith, 1998: Crop evapotranspiration—Guidelines for computing crop water requirements. *FAO Irrigation and Drainage Paper* **56**, 300 pp., https://www.fao.org/3/x0490e/x0490e00.htm.

Arnault, J., R. Knoche, J. Wei, and H. Kunstmann, 2016: Evaporation tagging and atmospheric water budget analysis with WRF: A regional precipitation recycling study for West Africa. *Water Resour. Res.*, **52**, 1544–1567, https://doi.org/10.1002/2015WR017704.

——, and Coauthors, 2021: Lateral terrestrial water flow contribution to summer precipitation at continental scale—A comparison between Europe and West Africa with WRF-Hydro-tag ensembles. *Hydrol. Processes*, **35**, e14183, https://doi.org/10.1002/hyp.14183.

Balog, I., Z. Podrascanin, F. Spinelli, G. Caputo, R. Siviero, and A. Benedetti, 2019: Hourly forecast of solar radiation up to 48h with two runs of weather research forecast model over Italy. *AIP Conf. Proc.*, **2126**, 190004, https://doi.org/10.1063/1.5117701.

Batista, G. E., and M. C. Monard, 2003: An analysis of four missing data treatment methods for supervised learning. *Appl. Artif. Intell.*, **17**, 519–533, https://doi.org/10.1080/713827181.

Bessah, E., and Coauthors, 2022: Climatic zoning of Ghana using selected meteorological variables for the period 1976–2018. *Meteor. Appl.*, **29**, e2049, https://doi.org/10.1002/met.2049.

Bliefernicht, J., and Coauthors, 2018: The WASCAL hydrometeorological observatory in the Sudan savanna of Burkina Faso and Ghana. *Vadose Zone J.*, **17**, 1–20, https://doi.org/10.2136/vzj2018.03.0065.

——, M. Waongo, S. Salack, J. Seidel, P. Laux, and H. Kunstmann, 2019: Quality and value of seasonal precipitation forecasts issued by the West African regional climate outlook forum. *J. Appl. Meteor. Climatol.*, **58**, 621–642, https://doi.org/10.1175/JAMC-D-18-0066.1.

BSRN, 2021: Baseline Surface Radiation Network. World Radiation Monitoring Center, https://bsrn.awi.de/.

Chen, W.-D., F. Cui, H. Zhou, H. Ding, and D.-X. Li, 2017: Impacts of different radiation schemes on the prediction of solar radiation and photovoltaic power. *Atmos. Oceanic Sci. Lett.*, **10**, 446–451, https://doi.org/10.1080/16742834.2017.1394780.

Cheng, X., D. Ye, Y. Shen, D. Li, and J. Feng, 2022: Studies on the improvement of modelled solar radiation and the attenuation effect of aerosol using the WRF-Solar model with satellite-based AOD data over north China. *Renewable Energy*, **196**, 358–365, https://doi.org/10.1016/j.renene.2022.06.141.

Danso, D. K., S. Anquetin, A. Diedhiou, K. Kouadio, and A. T. Kobea, 2020: Daytime low-level clouds in West Africa—Occurrence, associated drivers, and shortwave radiation attenuation. *Earth Syst. Dyn.*, **11**, 1133–1152, https://doi.org/10.5194/esd-11-1133-2020.

Deng, A., B. Gaudet, J. Dudhia, and K. Alapaty, 2014: Implementation and evaluation of a new shallow convection scheme in WRF. *26th Conf. on Weather Analysis and Forecasting/22nd Conf. on Numerical Weather Prediction*, Atlanta, GA, Amer. Meteor. Soc., 12.5, https://ams.confex.com/ams/94Annual/webprogram/Manuscript/Paper236925/12%205_22nd_NWP_Conf_Deng_ExtendedAbstract.pdf.

Dike, V. N., and Coauthors, 2018: Obstacles facing Africa's young climate scientists. *Nat. Climate Change*, **8**, 447–449, https://doi.org/10.1038/s41558-018-0178-x.

Dommo, A., D. A. Vondou, N. Philippon, R. Eastman, V. Moron, and N. Aloysius, 2022: The ERA5's diurnal cycle of low-level clouds over western central Africa during June–September: Dynamic and thermodynamic processes. *Atmos. Res.*, **280**, 106426, https://doi.org/10.1016/j.atmosres.2022.106426.

Flamant, C., and Coauthors, 2018: The Dynamics–Aerosol–Chemistry–Cloud Interactions in West Africa Field Campaign: Overview and research highlights. *Bull. Amer. Meteor. Soc.*, **99**, 83–104, https://doi.org/10.1175/BAMS-D-16-0256.1.

Flemming, J., and Coauthors, 2015: Tropospheric chemistry in the integrated forecasting system of ECMWF. *Geosci. Model Dev.*, **8**, 975–1003, https://doi.org/10.5194/gmd-8-975-2015.

Gamarro, H., J. E. Gonzalez, and L. E. Ortiz, 2019: On the assessment of a numerical weather prediction model for solar photovoltaic power forecasts in cities. *J. Energy Resour. Technol.*, **141**, 061203, https://doi.org/10.1115/1.4042972.

Gbode, I. E., J. Dudhia, K. O. Ogunjobi, and V. O. Ajayi, 2019: Sensitivity of different physics schemes in the WRF Model during a West African monsoon regime. *Theor. Appl. Climatol.*, **136**, 733–751, https://doi.org/10.1007/s00704-018-2538-x.

Gueye, M., and G. S. Jenkins, 2019: Investigating the sensitivity of the WRF-Chem horizontal grid spacing on PM_{10} concentration during 2012 over West Africa. *Atmos. Environ.*, **196**, 152–163, https://doi.org/10.1016/j.atmosenv.2018.09.064.

Gueymard, C. A., and P. A. Jimenez, 2018: Validation of real-time solar irradiance simulations over Kuwait using WRF-Solar. *12th Int. Conf. on Solar Energy for Buildings and Industry*, Rapperswil, Switzerland, International Solar Energy Society, https://doi.org/10.18086/eurosun2018.09.14.

Hannak, L., P. Knippertz, A. H. Fink, A. Kniffka, and G. Pante, 2017: Why do global climate models struggle to represent low-level clouds in the West African summer monsoon? *J. Climate*, **30**, 1665–1687, https://doi.org/10.1175/JCLI-D-16-0451.1.

Hersbach, H., and Coauthors, 2020: The ERA5 global reanalysis. *Quart. J. Roy. Meteor. Soc.*, **146**, 1999–2049, https://doi.org/10.1002/qj.3803.

Hill, P. G., R. P. Allan, J. C. Chiu, A. Bodas-Salcedo, and P. Knippertz, 2018: Quantifying the contribution of different cloud types to the radiation budget in southern West Africa. *J. Climate*, **31**, 5273–5291, https://doi.org/10.1175/JCLI-D-17-0586.1.

Hong, S.-Y., and J. Dudhia, 2012: Next-generation numerical weather prediction: Bridging parameterization, explicit clouds, and large eddies. *Bull. Amer. Meteor. Soc.*, **93**, ES6–ES9, https://doi.org/10.1175/2011BAMS3224.1.

IEA, 2018: Recent trends in solar PV. https://www.iea.org/tcep/power/renewables/solar/.

Inness, A., and Coauthors, 2019: The CAMS reanalysis of atmospheric composition. *Atmos. Chem. Phys.*, **19**, 3515–3556, https://doi.org/10.5194/acp-19-3515-2019.

Jiménez, P. A., S. Alessandrini, S. E. Haupt, A. Deng, B. Kosovic, J. A. Lee, and L. Delle Monache, 2016a: The role of unresolved clouds on short-range global horizontal irradiance predictability. *Mon. Wea. Rev.*, **144**, 3099–3107, https://doi.org/10.1175/MWR-D-16-0104.1.

——, and Coauthors, 2016b: WRF-Solar: Description and clear-sky assessment of an augmented NWP model for solar power prediction. *Bull. Amer. Meteor. Soc.*, **97**, 1249–1264, https://doi.org/10.1175/BAMS-D-14-00279.1.

——, J. Yang, J.-H. Kim, M. Sengupta, and J. Dudhia, 2022: Assessing the WRF-Solar model performance using satellite-derived irradiance from the National Solar Radiation Database. *J. Appl. Meteor. Climatol.*, **61**, 129–142, https://doi.org/10.1175/JAMC-D-21-0090.1.

Kim, J.-Y., C.-Y. Yun, C. K. Kim, Y.-H. Kang, H.-G. Kim, S.-N. Lee, and S.-Y. Kim, 2017: Evaluation of WRF Model-derived direct irradiance for solar thermal resource assessment over South Korea. *AIP Conf. Proc.*, **1850**, 140013, https://doi.org/10.1063/1.4984521.

Klein, C., D. Heinzeller, J. Bliefernicht, and H. Kunstmann, 2015: Variability of West African monsoon patterns generated by a WRF multi-physics ensemble. *Climate Dyn.*, **45**, 2733–2755, https://doi.org/10.1007/s00382-015-2505-5.

Knippertz, P., A. H. Fink, R. Schuster, J. Trentmann, J. M. Schrage, and C. Yorke, 2011: Ultra-low clouds over the southern West African monsoon region. *Geophys. Res. Lett.*, **38**, L21808, https://doi.org/10.1029/2011GL049278.

Kumi, E. N., 2017: The electricity situation in Ghana: Challenges and opportunities. Center for Global Development Policy Paper, 30 pp., https://www.cgdev.org/sites/default/files/electricity-situation-ghana-challenges-and-opportunities.pdf.

Kuye, A., and S. S. Jagtap, 1992: Analysis of solar radiation data for Port Harcourt, Nigeria. *Sol. Energy*, **49**, 139–145, https://doi.org/10.1016/0038-092X(92)90148-4.

Lara-Fanego, V., J. A. Ruiz-Arias, D. Pozo-Vázquez, F. J. Santos-Alamillos, and J. Tovar-Pescador, 2012: Evaluation of the WRF model solar irradiance forecasts in Andalusia (southern Spain). *Sol. Energy*, **86**, 2200–2217, https://doi.org/10.1016/j.solener.2011.02.014.

Lee, L. A., C. L. Reddington, and K. S. Carslaw, 2016: On the relationship between aerosol model uncertainty and radiative forcing uncertainty. *Proc. Natl. Acad. Sci. USA*, **113**, 5820–5827, https://doi.org/10.1073/pnas.1507050113.

Legates, D. R., and G. J. McCabe, 2013: A refined index of model performance: A rejoinder. *Int. J. Climatol.*, **33**, 1053–1056, https://doi.org/10.1002/joc.3487.

Léon, J.-F., A. B. Akpo, M. Bedou, J. Djossou, M. Bodjrenou, V. Yoboué, and C. Liousse, 2021: PM$_{2.5}$ surface concentrations in southern West African urban areas based on sun photometer and satellite observations. *Atmos. Chem. Phys.*, **21**, 1815–1834, https://doi.org/10.5194/acp-21-1815-2021.

Liu, Y., Y. Qian, S. Feng, L. K. Berg, T. W. Juliano, P. A. Jiménez, and Y. Liu, 2022: Sensitivity of solar irradiance to model parameters in cloud and aerosol treatments of WRF-solar. *Sol. Energy*, **233**, 446–460, https://doi.org/10.1016/j.solener.2022.01.061.

Naabil, E., B. L. Lamptey, J. Arnault, A. Olufayo, and H. Kunstmann, 2017: Water resources management using the WRF-Hydro modelling system: Case-study of the Tono dam in West Africa. *J. Hydrol. Reg. Stud.*, **12**, 196–209, https://doi.org/10.1016/j.ejrh.2017.05.010.

Neher, I., T. Buchmann, S. Crewell, B. Pospichal, and S. Meilinger, 2019: Impact of atmospheric aerosols on solar power. *Meteor. Z.*, **28**, 305–321, https://doi.org/10.1127/metz/2019/0969.

Neill, S. P., and M. R. Hashemi, 2018: Ocean modelling for resource characterization. *Fundamentals of Ocean Renewable Energy*, S. P. Neill and M. R. Hashemi, Eds., Academic Press, 193–235, https://doi.org/10.1016/B978-0-12-810448-4.00008-2.

Nicholson, S. E., 1981: Rainfall and atmospheric circulation during drought periods and wetter years in West Africa. *Mon. Wea. Rev.*, **109**, 2191–2208, https://doi.org/10.1175/1520-0493(1981)109<2191:RAACDD>2.0.CO;2.

——, A. H. Fink, and C. Funk, 2018: Assessing recovery and change in West Africa's rainfall regime from a 161-year record. *Int. J. Climatol.*, **38**, 3770–3786, https://doi.org/10.1002/joc.5530.

Niu, G.-Y., and Coauthors, 2011: The community Noah land surface model with multiparameterization options (Noah-MP): 1. Model description and evaluation with local-scale measurements. *J. Geophys. Res.*, **116**, D12109, https://doi.org/10.1029/2010JD015139.

Noble, E., L. M. Druyan, and M. Fulakeza, 2014: The sensitivity of WRF daily summertime simulations over West Africa to alternative parameterizations. Part I: African wave circulation. *Mon. Wea. Rev.*, **142**, 1588–1608, https://doi.org/10.1175/MWR-D-13-00194.1.

Okogbue, E. C., J. A. Adedokun, and B. Holmgren, 2009: Hourly and daily clearness index and diffuse fraction at a tropical station, Ile-Ife, Nigeria. *Int. J. Climatol.*, **29**, 1035–1047, https://doi.org/10.1002/joc.1849.

Olson, J. B., J. S. Kenyon, W. A. Angevine, J. M. Brown, M. Pagowski, and K. Sušelj, 2019: A description of the MYNN-EDMF scheme and the coupling to other components in WRF-ARW. NOAA Tech. Memo. OAR GSD 61, 42 pp., https://doi.org/10.25923/n9wm-be49.

Oluleye, A., and A. Folorunsho, 2019: Influence of atmospheric dynamic factors on dust aerosol mobilization over West Africa: Simulations from WRF-Chem. *Aerosol Sci. Eng.*, **3**, 132–149, https://doi.org/10.1007/s41810-019-00048-z.

Pedruzo-Bagazgoitia, X., P. A. Jiménez, J. Dudhia, and J. V.-G. de Arellano, 2019: Shallow cumulus representation and its interaction with radiation and surface at the convection gray zone. *Mon. Wea. Rev.*, **147**, 2467–2483, https://doi.org/10.1175/MWR-D-19-0030.1.

Peuch, V.-H., and Coauthors, 2018: The use of satellite data in the Copernicus Atmosphere Monitoring Service (CAMS). *IGARSS 2018—2018 IEEE Int. Geoscience and Remote Sensing Symp.*, Valencia, Spain, Institute of Electrical and Electronics Engineers, 1594–1596, https://doi.org/10.1109/IGARSS.2018.8518698.

Prasad, A. A., and M. Kay, 2020: Assessment of simulated solar irradiance on days of high intermittency using WRF-Solar. *Energies*, **13**, 385, https://doi.org/10.3390/en13020385.

Quaas, J., and Coauthors, 2009: Aerosol indirect effects—General circulation model intercomparison and evaluation with satellite data. *Atmos. Chem. Phys.*, **9**, 8697–8717, https://doi.org/10.5194/acp-9-8697-2009.

Quenum, G. M. L. D., J. Arnault, N. A. Klutse, P. Oguntunde, and H. Kunstmann, 2020: Potential of the coupled WRF-Hydro modeling system for flood forecasting in the Ouémé-river basin (Benin, West Africa): An assessment with the stochastic kinetic-energy backscatter scheme. Authorea Preprints, 10 pp., https://doi.org/10.22541/au.160921196.60045253/v1.

Ruiz-Arias, J. A., J. Dudhia, F. J. Santos-Alamillos, and D. Pozo-Vázquez, 2013: Surface clear-sky shortwave radiative closure intercomparisons in the Weather Research and Forecasting Model. *J. Geophys. Res. Atmos.*, **118**, 9901–9913, https://doi.org/10.1002/jgrd.50778.

——, ——, and C. A. Gueymard, 2014: A simple parameterization of the short-wave aerosol optical properties for surface direct and diffuse irradiances assessment in a numerical weather model. *Geosci. Model Dev.*, **7**, 1159–1174, https://doi.org/10.5194/gmd-7-1159-2014.

——, C. Arbizu-Barrena, F. J. Santos-Alamillos, J. Tovar-Pescador, and D. Pozo-Vázquez, 2016: Assessing the surface solar radiation budget in the WRF Model: A spatiotemporal analysis of the bias and its causes. *Mon. Wea. Rev.*, **144**, 703–711, https://doi.org/10.1175/MWR-D-15-0262.1.

Salack, S., and Coauthors, 2019: Designing transnational hydroclimatological observation networks and data sharing policies in West Africa. *Data Sci. J.*, **18**, 1–15, https://doi.org/10.5334/dsj-2019-033.

Sawadogo, W., B. J. Abiodun, and E. C. Okogbue, 2020: Impact of global warming on photovoltaic power generation over West Africa. *Renewable Energy*, **151**, 263–277, https://doi.org/10.1016/j.renene.2019.11.032.

——, and Coauthors, 2022: Hourly global horizontal irradiance over West Africa: Satellite- and reanalysis-derived estimates vs. in situ measurements. SSRN, 4152712, https://doi.org/10.2139/ssrn.4152712.

Schrage, J. M., and A. H. Fink, 2012: Nocturnal continental low-level stratus over tropical West Africa: Observations and possible mechanisms controlling its onset. *Mon. Wea. Rev.*, **140**, 1794–1809, https://doi.org/10.1175/MWR-D-11-00172.1.

Schuster, G. L., O. Dubovik, and B. N. Holben, 2006: Angstrom exponent and bimodal aerosol size distributions. *J. Geophys. Res.*, **111**, D07207, https://doi.org/10.1029/2005JD006328.

Sosa-Tinoco, I., M. A. Prósper, and G. Miguez-Macho, 2022: Development of a solar energy forecasting system for two real solar plants based on WRF Solar with aerosol input and a solar plant model. *Sol. Energy*, **240**, 329–341, https://doi.org/10.1016/j.solener.2022.05.049.

Sylla, M. B., N. Elguindi, F. Giorgi, and D. Wisser, 2016: Projected robust shift of climate zones over West Africa in response to anthropogenic climate change for the late 21st century. *Climatic Change*, **134**, 241–253, https://doi.org/10.1007/s10584-015-1522-z.

Thompson, G., and T. Eidhammer, 2014: A study of aerosol impacts on clouds and precipitation development in a large winter cyclone. *J. Atmos. Sci.*, **71**, 3636–3658, https://doi.org/10.1175/JAS-D-13-0305.1.

——, M. Tewari, K. Ikeda, S. Tessendorf, C. Weeks, J. Otkin, and F. Kong, 2016: Explicitly-coupled cloud physics and radiation parameterizations and subsequent evaluation in WRF high-resolution convective forecasts. *Atmos. Res.*, **168**, 92–104, https://doi.org/10.1016/j.atmosres.2015.09.005.

Troccoli, A., and J. J. Morcrette, 2014: Skill of direct solar radiation predicted by the ECMWF global atmospheric model over Australia. *J. Appl. Meteor. Climatol.*, **53**, 2571–2588, https://doi.org/10.1175/JAMC-D-14-0074.1.

U.S. Agency for International Development, 2020: Ghana Power Africa fact sheet. https://www.usaid.gov/powerafrica/ghana.

Verbois, H., R. Huva, A. Rusydi, and W. Walsh, 2018: Solar irradiance forecasting in the tropics using numerical weather prediction and statistical learning. *Sol. Energy*, **162**, 265–277, https://doi.org/10.1016/j.solener.2018.01.007.

Wilks, D. S., 2011: *Statistical Methods in the Atmospheric Sciences.* 3rd ed. Elsevier, 676 pp.

Xia, Y., and Coauthors, 2022: Concurrent hot extremes and high ultraviolet radiation in summer over the Yangtze Plain and their possible impact on surface ozone. *Environ. Res. Lett.*, **17**, 064001, https://doi.org/10.1088/1748-9326/ac6c3c.

Xie, Y., M. Sengupta, and J. Dudhia, 2016: A Fast All-Sky Radiation Model for Solar Applications (FARMS): Algorithm and performance evaluation. *Sol. Energy*, **135**, 435–445, https://doi.org/10.1016/j.solener.2016.06.003.

Yang, J., J.-H. Kim, P. A. Jiménez, M. Sengupta, J. Dudhia, Y. Xie, A. Golnas, and R. Giering, 2021: An efficient method to identify uncertainties of WRF-Solar variables in forecasting solar irradiance using a tangent linear sensitivity analysis. *Sol. Energy*, **220**, 509–522, https://doi.org/10.1016/j.solener.2021.03.044.

Zempila, M.-M., T. M. Giannaros, A. Bais, D. Melas, and A. Kazantzidis, 2016: Evaluation of WRF shortwave radiation parameterizations in predicting global horizontal irradiance in Greece. *Renewable Energy*, **86**, 831–840, https://doi.org/10.1016/j.renene.2015.08.057.